

expression in mice with a targeted deletion in p53. Basal SIRT1 expression was higher in adipose tissue of p53^{-/-} mice than in wild-type controls (Fig. 4A). This result is particularly interesting given the recent observation that SIRT1 plays a prominent role in fat usage (15). A survey of other tissues revealed a more modest but consistent increase in basal SIRT1 expression in the p53^{-/-} mice (fig. S9). However, *SIRT1* mRNA did not appreciably change in either liver or skeletal muscle of p53^{-/-} mice after overnight fasting (Figs. 1F and 4B). This lack of starvation-induced SIRT1 expression occurred even though, relative to wild-type animals, p53^{-/-} mice had an even greater drop in their fasting glucose after food withdrawal (wild-type mice, 102 ± 7 mg/dl; p53^{-/-} mice, 76 ± 8 mg/dl; n = 4 each, P < 0.01). These in vivo results further support a role for p53 in SIRT1 regulation.

Our results show that in mammalian cells, a simple model of acute nutritional stress results in a Foxo3a-dependent increase in SIRT1 levels. Interestingly, chronic caloric restriction also increases SIRT1 expression (16). Foxo3a regulation of SIRT1 expression occurs through an interaction

with p53. In this regard, it is interesting to note that Forkhead proteins and p53 share a number of similarities (14, 17). In the worm, Forkhead proteins respond to nutrient availability and a homolog of p53 regulates starvation response (18). In mammals, although p53 is often linked to cancer and Forkhead proteins are commonly associated with aging, recent evidence has suggested a role for Forkhead proteins in tumorigenesis (19, 20) and a role for p53 in life-span (21, 22). Finally, both Foxo3a and p53 directly and independently bind to SIRT1 (6, 7, 23, 24). Taken together, these results suggest a complicated but undoubtedly important homeostatic regulatory network involving p53, Foxo3a, and SIRT1. Further analysis of this network may help us to understand how adaptation to certain cellular stresses, including nutrient availability, may modulate mammalian life-span.

References and Notes

1. M. Keiberlein, M. McVey, L. Guarente, *Genes Dev.* **13**, 2570 (1999).
2. H. A. Tissenbaum, L. Guarente, *Nature* **410**, 227 (2001).
3. S. J. Lin, P. A. Defossez, L. Guarente, *Science* **289**, 2126 (2000).
4. G. I. Patterson, *Curr. Biol.* **13**, R279 (2003).

5. S. T. Henderson, T. E. Johnson, *Curr. Biol.* **11**, 1975 (2001).
6. M. C. Motta et al., *Cell* **116**, 551 (2004).
7. A. Brunet et al., *Science* **303**, 2011 (2003).
8. See supporting data on Science Online.
9. D. Durocher, J. Henkel, A. R. Fersht, S. P. Jackson, *Mol. Cell* **4**, 387 (1999).
10. D. Durocher et al., *Mol. Cell* **6**, 1169 (2000).
11. G. S. Stewart et al., *Nature* **421**, 961 (2003).
12. Z. Lou, K. Minter-Dykhouse, X. Wu, J. Chen, *Nature* **421**, 957 (2003).
13. J. Falck et al., *Oncogene* **20**, 5503 (2001).
14. M. Oren, *Cell Death Differ.* **10**, 431 (2003).
15. F. Picard et al., *Nature* **429**, 771 (2004).
16. H. Y. Cohen et al., *Science* **305**, 390 (2004).
17. B. M. Burgering, G. J. Kops, *Trends Biochem. Sci.* **27**, 352 (2002).
18. W. B. Derry, A. P. Putzke, J. H. Rothman, *Science* **294**, 591 (2001).
19. M. C. T. Hu et al., *Cell* **117**, 225 (2004).
20. J. Seoane et al., *Cell* **117**, 211 (2004).
21. S. D. Tyner et al., *Nature* **415**, 45 (2002).
22. B. Maier et al., *Genes Dev.* **18**, 306 (2004).
23. J. Luo et al., *Cell* **107**, 137 (2001).
24. H. Vaziri et al., *Cell* **107**, 149 (2001).
25. We thank I. Rovira for help in preparing this manuscript. Supported by NHLBI Intramural Funds.

Supporting Online Material

www.sciencemag.org/cgi/content/full/306/5704/2105/DC1

Materials and Methods

Figs. S1 to S9

References

21 June 2004; accepted 1 November 2004
10.1126/science.1101731

Cofolding Organizes Alfalfa Mosaic Virus RNA and Coat Protein for Replication

Laura M. Guogas,^{1,3} David J. Filman,²
James M. Hogle,^{2*} Lee Gehrke^{1,3*}

Alfalfa mosaic virus genomic RNAs are infectious only when the viral coat protein binds to the RNA 3' termini. The crystal structure of an alfalfa mosaic virus RNA-peptide complex reveals that conserved AUGC repeats and Pro-Thr-x-Arg-Ser-x-x-Tyr coat protein amino acids cofold upon interacting. Alternating AUGC residues have opposite orientation, and they base pair in different adjacent duplexes. Localized RNA backbone reversals stabilized by arginine-guanine interactions place the adenosines and guanines in reverse order in the duplex. The results suggest that a uniform, organized 3' conformation, similar to that found on viral RNAs with transfer RNA-like ends, may be essential for replication.

A general problem in positive-strand RNA virology is understanding how viral RNA replication is initiated by the RNA-dependent RNA polymerase (replicase) on the correct template and nucleotide in an infected cell.

Alfalfa mosaic virus (AMV) and ilarviruses are unusual positive-sense viruses, the genomic RNAs of which are replicated only in the presence of the viral coat protein (CP) (1, 2). These viruses are distinguished from many other members of the virus family *Bromoviridae* because they lack canonical features of the tRNA-like structure (TLS) common at the 3' termini of the viral RNA genomes. The TLS is a necessary and sufficient feature for recruitment of the bromovirus replicase (3, 4). CP-induced structural organization of the AMV RNA 3' terminus may create a functional homolog of the

tRNA tail and thereby permit recognition by the RNA-dependent RNA polymerase.

CP binds specifically to the 3' untranslated regions (3'UTRs) found on all four RNAs of the segmented AMV genome (5). The 180-nucleotide 3'UTR secondary structure likely consists of six hairpins, most of which are separated by single-stranded tetranucleotide AUGC repeats (5–8). These repeats are characteristic of AMV and ilarvirus RNA sequences and are important for CP binding (8–11). We previously identified a 39-nucleotide minimal high affinity AMV CP-binding site, consisting of the two terminal hairpins and their flanking AUGC nucleotides (nucleotides 843 to 881 in RNA4; i.e., AMV_{843–881}) (8, 12, 13) (fig. S1A). This fragment is competent to bind either full-length CP or a 26-amino acid peptide (CP26, fig. S1B) (13) representing the N-terminal RNA binding domain (14). The CP N terminus contains a Pro-Thr-x-Arg-Ser-x-x-Tyr (PTxRSxxY) RNA binding domain conserved among AMV and ilarvirus CPs (14). The arginine at position 17 is critical for both RNA binding and virus replication (14–16). Circular dichroism experiments suggest that the CP N terminus is unstructured in solution (17). Previous virus crystallization attempts required proteolytic cleavage of the AMV CP N terminus (18, 19).

Crystals of the AMV N-terminal CP peptide CP26 in complex with 5-bromouridine-labeled AMV_{843–881} RNA were grown in hanging drops by vapor diffusion. The structure was

¹Department of Microbiology and Molecular Genetics, ²Department of Biological Chemistry and Molecular Pharmacology, Harvard Medical School, Boston, MA 02115, USA. ³Harvard-MIT Division of Health Sciences and Technology, Massachusetts Institute of Technology, Cambridge, MA 02139, USA.

*To whom correspondence should be addressed. E-mail: Lee_Gehrke@hms.harvard.edu (L.G.); James_Hogle@hms.harvard.edu (J.M.H.)

solved to 3.0 Å resolution with phases obtained by multiple-wavelength anomalous dispersion (table S1) (13). The cocrystal structure reveals that the RNA and peptides undergo cofolding events that substantially alter their structure from their unbound forms. The RNA forms two hairpins oriented at approximately right angles (Fig. 1A). Each of the RNA hairpins is extended by two base pairs formed between nucleotides from adjacent AUGC sequences (Figs. 1 and 2). Loop nucleotides could not be placed into the final model (fig. S2) (13). The two CP26 peptides each form an α helix with an extended N-terminal tail (Fig. 1A). Residues 12 to 26 are ordered in peptide 1, whereas residues 9 to 26 are ordered in peptide 2. The extreme N termini of both peptides remained flexible and were not visible.

A notable feature of the structure is that cofolding events promote base pairing between the AUGC repeats in the presence of CP. The U(844) and C(846) nucleotides pair with A(865) and G(867), respectively, at the base of duplex 1 (Figs. 1C and 2A). The C=G pair is a Watson-Crick pair, whereas the A-U pair is a noncanonical UA reverse Watson-Crick pair. An identical interaction is seen at the base of duplex 2, which is extended by two base pairs when U(866) and C(868) hydrogen bond with A(878) and G(880), respectively (Figs. 1C and 2B). The formation of these base pairs introduces two types of distortion into the AMV RNA. First, the interhelical AUGC₈₆₅₋₈₆₈ (purple in Figs. 1 and 2) participates in base pairing interactions in both duplex 1 and duplex 2. This requires alternating bases of AUGC₈₆₅₋₈₆₈ to be oriented in opposite directions. Second, to form C=G base pairs, G(867) and G(880) must be positioned upstream of A(865) and A(878) in their respective stacks, out of numerical order (Fig. 1B). The insertion of G(867) and G(880) between A(864) and A(865) or G(877) and A(878), respectively, introduces an unusual kink into the ribose-phosphate backbone (Fig. 1). In duplex 1, A(864) and A(865) are separated by the insertion of G(867) into the base stack. U(866) is flipped out of the base stack of duplex 1 and instead participates in reverse Watson-Crick base pairing at the base of duplex 2 (Fig. 2A). The same interaction is seen at the base of duplex 2 (Fig. 2B), where the distance between G(877) and A(878) is also increased to accommodate the insertion of G(880) between them to form a base pair with C(868).

Amino acids in the conserved RNA binding motif PTxRSxxY play key roles in stabilizing the AUGC base pairing interactions. Biochemical evidence suggesting the importance of arginine 17 (14) is consistent with its central position within the RNA protein-binding site. Both the G(867)-C(846)

and G(880)-C(868) base pairs are displaced from the helical axis toward the minor groove, allowing the Arg¹⁷ sidechain guanidinium to insert into the base stack at the major groove. Arg¹⁷ is positioned to make polydentate hydrogen bonds with the G(867) (peptide 1) and G(880) (peptide 2) bases, thus extending the stacking interaction of the guanine bases with A(865) and A(878), respectively (Fig. 3A). The importance of arginine residues in RNA-peptide interactions was demonstrated previously in the human immunodeficiency virus Tat/Tar complex (20). The bottoms of both hairpins are capped by conserved tyrosine (Tyr²¹) sidechains from peptides 1 and 2. Between Arg¹⁷ and Pro¹⁴, both copies of the CP26 peptide

transition from α helix to extended chain. This transition is mediated by a tight turn between Thr¹⁵ and Pro¹⁴, forming an L shape that cradles the extended RNA duplex (Fig. 1A). The L turn allows the N-terminal tail of peptide 2 to straddle a groove in the RNA surface formed by duplex 1 and duplex 2, and to make additional contacts between the RNA backbone of duplex 1 and Lys¹³ and Gln¹⁹ of peptide 2 (Fig. 1B). This conformation is facilitated by the conserved Pro¹⁴ and is stabilized by an exchange of hydrogen bonds between the sidechain hydroxyls and the mainchain amides of Thr¹⁵ and Ser¹⁸ within the PTxRSxxY motifs (Fig. 3B). The side chain of Ser¹⁸ occupies a pocket that provides an optimal fit. It forms hydrogen

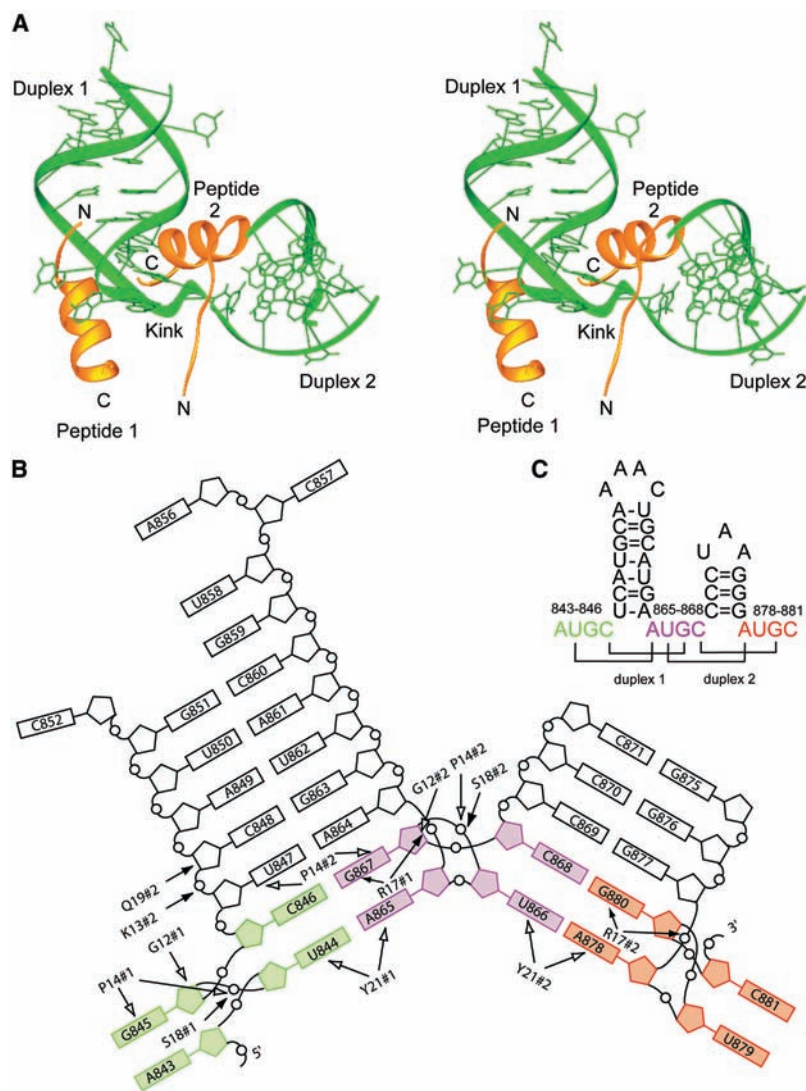


Fig. 1. (A) Stereoview of the AMV RNA-CP complex. The RNA is shown in green and the CP26 peptides are shown in gold. (B) Schematic diagram of the AMV RNA and CP26 protein contacts. The AUGC sequences have been color coded. The 5' AUGC is colored green, the interhelical AUGC sequence is colored purple, and the 3' AUGC sequence is colored red. Hydrogen-bonding contacts between the RNA and peptide are indicated with filled arrows and van der Waals contacts are indicated by open arrows. #1, peptide 1; #2, peptide 2; G, Gly; K, Lys; P, Pro; Q, Gln; R, Arg; S, Ser; Y, Tyr. (C) Secondary structure of the 39-nucleotide minimal binding domain found at the 3' end of AMV RNAs, AMV₈₄₃₋₈₈₁. The AUGC sequences are color coded as in (B). Base pairs are indicated by brackets.

bonds with the phosphate oxygen of G(845) (peptide 1) or G(867) (peptide 2) and the amide nitrogen of Thr¹⁵ (Fig. 3B). Pro¹⁴ makes van der Waals contacts with the ribose ring and phosphate oxygen of G(845) (peptide 1) and G(867) (peptide 2) (Fig. 1B). The edge of the Pro¹⁴ sidechain makes additional favorable packing contacts with the ribose-phosphate backbone above and below the plane of the proline ring, contributing to the stability of the complex. Mutation of Pro¹⁴, Ser¹⁸, or Tyr²¹ diminishes CP26-AMV₈₄₃₋₈₈₁ RNA binding affinity and replication activity (21), underscoring the importance of these contacts for the stability of the RNA-protein complex.

The structure correlates well with biochemical and functional data. Disruption of either the CP-binding site on the RNA or the RNA binding site on the CP prevents formation of the complex and blocks RNA replication (12, 15-17, 22). The contacts related to the L turn, which were not predicted by amino acid sequence homology, provide a structural basis for the observed protection of nucleotides 847 to 850 during hydroxyl radical footprinting experiments (8, 12). In vitro RNA selection experiments (10, 11) and hydroxyl radical footprinting data (8, 14) suggested that peptides bind to the base of the hairpins without substantial loop interactions. The inter-AUGC base pairing contacts are consistent with previous chemical modification data and in vitro selection showing that modification of U(844) or C(846) diminished CP binding (12), whereas degenerate in vitro selection data show the strong conservation of nucleotide identity at the AUGC positions (11). The importance of the central AUGC and the dual hairpin contacts made in this region with peptide 2 (Fig. 1) was also anticipated on the basis of biochemical data revealing that peptide binding was abolished if tandem AUGC repeats separated the two hairpins (23).

The unusual inter-AUGC base pairing seen in the structure and the conservation of AUGC sequences among AMV and ilarvirus 3'UTRs (fig. S3A) prompted us to test whether CP can bind RNAs containing nucleotide substitutions that preserve base pairing, even though the substitutions are not strictly structurally equivalent. We changed all three AUGC sequences in AMV₈₄₃₋₈₈₁ to CGUA, GCAU, or UACG. None of these RNAs bound CP26 in mobility shift assays (fig. S3B) (13). The positions of G(867) and G(880) are likely to be critical for CP binding because of their close interaction with the critical Arg¹⁷ residue. An additional UAGC mutant, designed to leave the position of the C=G base pair unchanged, also did not bind CP26. This observation is consistent with the proposal that the extended stacking of Arg¹⁷-G(867) and Arg¹⁷-G(880) with

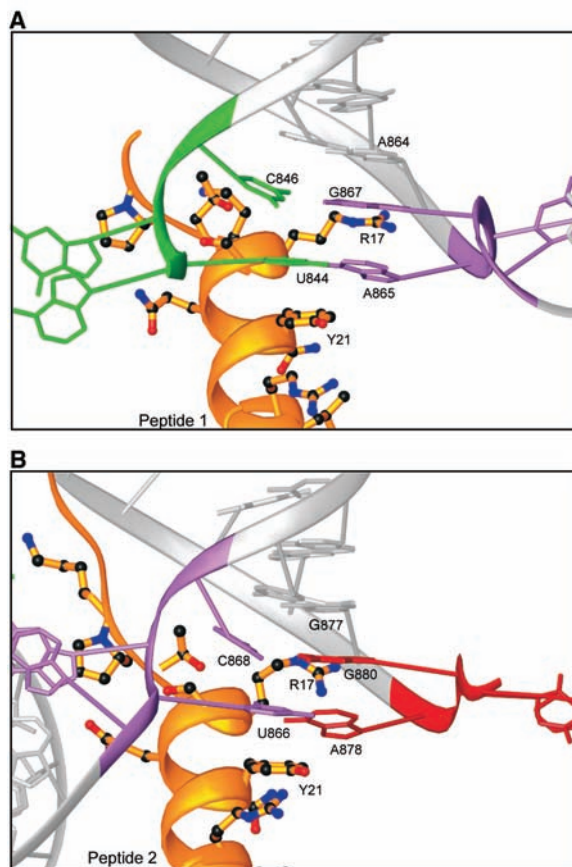
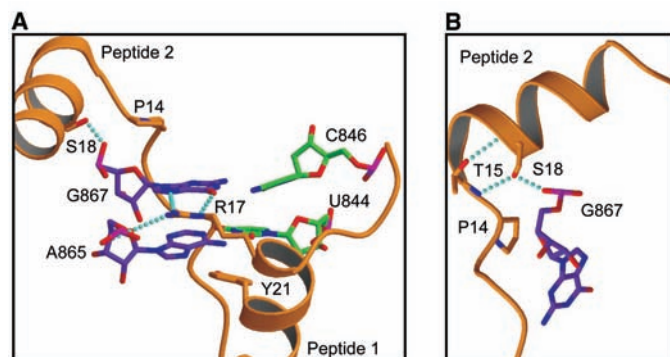


Fig. 2. Formation of inter-AUGC base pairs. (A) RNA-peptide interactions at the base of duplex 1. The CP peptide α helix and sidechains are shown in gold. The RNA is shown in gray. The 5' AUGC sequence is colored green, and the interhelical AUGC sequence is colored purple. (B) Similar RNA-peptide interactions are seen at the base of duplex 2. The interhelical AUGC sequence is highlighted in purple and the 3' AUGC sequence is colored red. R, Arg; Y, Tyr.

Fig. 3. Interactions between the AMV RNA and CP26 peptides. (A) View of the two additional base pairs at the base of duplex 1 and their interaction with peptide sidechains. The carbon atoms of base pairing members at the base of duplex 1 from the 3' AUGC [U(844) and C(846)] are colored green, whereas members from the interhelical AUGC [A(865) and G(867)] are colored purple. Hydrogen bonds are indicated in cyan. (B) View of peptide 2 making the L-shaped turn. The carbon atoms of peptide 2 are colored gold, whereas those of G(867) are colored purple. P, Pro; R, Arg; S, Ser; T, Thr; Y, Tyr.

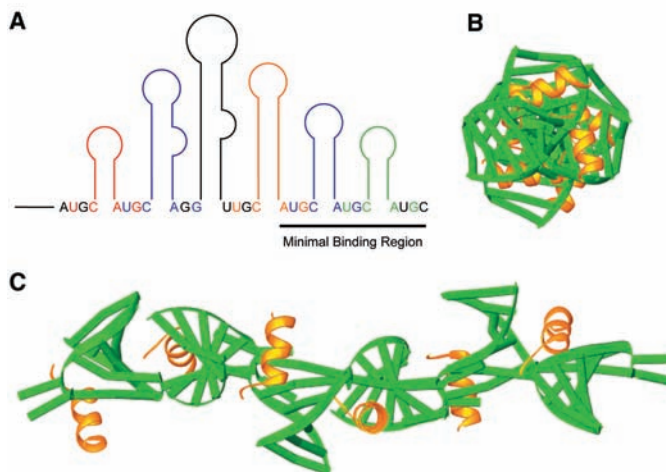


A(865) and A(878), respectively, contributes to the stability of the unusual base pair structure at the base of the stem loops.

Features of the AMV RNA-CP peptide complex may shed light on the mechanisms at work during the initial phases of virus replication. The structure suggests that the RNA assumes a highly ordered conformation in the presence of CP. The AUGC regions, single stranded and potentially flexible in the absence of CP (24), form base pairs when bound to CP26 and force the RNA to assume a more conformationally limited form. The recurring pattern of peptide interactions with duplex 1 and duplex 2 RNAs (Figs. 1B and

2) suggests that these types of contacts may also occur at other U-C-hairpin-A-G motifs throughout the 3'UTR (8) (Fig. 4A). We modeled CP binding along the entire length of the 3'UTR by aligning the AUGC regions of multiple copies of the AMV₈₄₃₋₈₈₁-CP26 structure, while ignoring the differing lengths of the hairpins. The resulting molecule forms a long rodlike structure with the hairpins projecting out from a central axis (Fig. 4, B and C). A transition from a more flexible to a more constrained 3' end upon CP binding agrees with a replication model suggesting that an RNA conformational change accompanies CP binding to the 3' ends of the

Fig. 4. Proposed structure of the entire 3'UTR. (A) Diagram of the 3'UTR with color-coded U-C-hairpin-A-G CP-binding sites. (B) End-on view of the simulated 3'UTR. (C) View of the 3'UTR along its length. RNA is colored green; peptide is colored yellow.



genomic RNAs (25). Circular dichroism analyses and polyacrylamide gel electrophoresis experiments also suggest that the AMV 3'UTR RNA becomes more compact in the presence of CP (11, 17). Sequential loading of CP along the length of the 3'UTR may specify switches between replication, translation, and assembly processes. As a general theme in nonpolyadenylated positive-strand RNA viruses, the structural organization of the extreme 3' terminus (here, by binding of two CP subunits at the base of the last two hairpins) may present a single conformation that is recognized by replicase enzymes. Organization of the entire length of the AMV 3'UTR (binding of CP molecules at the base of all hairpins) may specify assembly functions through the formation of a rodlike

structure to nucleate bacilliform particle formation.

References and Notes

1. J. F. Bol, L. van Vloten-Doting, E. M. Jaspars, *Virology* **46**, 73 (1971).
2. E. M. J. Jaspars, in *Molecular Plant Virology*, J. W. Davies, Ed. (CRC Press, New York, 1985), pp. 155–221.
3. T. W. Dreher, J. J. Bujarski, T. C. Hall, *Nature* **311**, 171 (1984).
4. M. R. Chapman, C. C. Kao, *J. Mol. Biol.* **286**, 709 (1999).
5. E. C. Koper-Zwarthoff, J. F. Bol, *Nucleic Acids Res.* **8**, 3307 (1980).
6. C. J. Houwing, E. M. Jaspars, *Biochemistry* **21**, 3408 (1982).
7. G. J. Quigley, L. Gehrke, D. A. Roth, P. E. Auron, *Nucleic Acids Res.* **12**, 347 (1984).
8. F. Houser-Scott, M. L. Baer, K. F. Liem Jr., J. M. Cai, L. Gehrke, *J. Virol.* **68**, 2194 (1994).
9. C. B. Reusken, L. Neeleman, J. F. Bol, *Nucleic Acids Res.* **22**, 1346 (1994).
10. F. Houser-Scott, P. Ansel-McKinney, J. M. Cai, L. Gehrke, *J. Virol.* **71**, 2310 (1997).

11. G. A. Rocheleau, J. E. Petrillo, L. M. Guogas, L. Gehrke, *J. Virol.* **78**, 8036 (2004).
12. P. Ansel-McKinney, L. Gehrke, *J. Mol. Biol.* **278**, 767 (1998).
13. Materials and methods are available as supporting material on Science Online.
14. P. Ansel-McKinney, S. W. Scott, M. Swanson, X. Ge, L. Gehrke, *EMBO J.* **15**, 5077 (1996).
15. V. M. Yusibov, L. S. Loesch-Fries, *Virology* **208**, 405 (1995).
16. V. Yusibov, L. S. Loesch-Fries, *Virology* **242**, 1 (1998).
17. M. L. Baer, F. Houser, L. S. Loesch-Fries, L. Gehrke, *EMBO J.* **13**, 727 (1994).
18. K. Fukuyama, S. S. Abdel-Meguid, J. E. Johnson, M. G. Rossmann, *J. Mol. Biol.* **167**, 873 (1983).
19. A. Kumar et al., *J. Virol.* **71**, 7911 (1997).
20. B. J. Calnan, B. Tidor, S. Biancalana, D. Hudson, A. D. Frankel, *Science* **252**, 1167 (1991).
21. J. E. Petrillo, L. M. Guogas, L. Gehrke, unpublished data.
22. C. B. Reusken, J. F. Bol, *Nucleic Acids Res.* **24**, 2660 (1996).
23. S. M. Laforest, L. Gehrke, *RNA* **10**, 48 (2004).
24. P. Ansel-McKinney, thesis, Harvard University (1996).
25. C. J. Houwing, E. M. Jaspars, *Biochemistry* **17**, 2927 (1978).
26. We thank S. Ginell and R. Zhang for support at beamline ID19 of the Advanced Photon Source (APS) and B. Appleton and T. Auperin for help with data collection. B. Eichman, T. Hollis, and E. Toth provided useful discussions and advice. Use of the Argonne National Laboratory Structural Biology Center beamlines at the APS was supported by the U.S. Department of Energy, Office of Energy Research, under Contract no. W-31-109-ENG-38. This work was supported by NIH awards GM42504 (L.G.) and AI20566 (J.H.) and by a fellowship from the Albert J. Ryan Foundation (L.M.G.). Structure factors and atomic coordinates have been deposited in the Protein Data Bank (accession number 1XOK).

Supporting Online Material

www.sciencemag.org/cgi/content/full/306/5704/2108/DC1
 Materials and Methods
 SOM Text
 Figs. S1 to S3
 Table S1
 References and Notes

29 July 2004; accepted 25 October 2004
 10.1126/science.1103399

bHLH Transcription Factor Olig1 Is Required to Repair Demyelinated Lesions in the CNS

Heather A. Arnett,^{1*} Stephen P. J. Fancy,^{2*} John A. Alberta,¹ Chao Zhao,² Sheila R. Plant,³ Sovann Kaing,¹ Cedric S. Raine,⁴ David H. Rowitch,¹ Robin J. M. Franklin,^{2,†} Charles D. Stiles^{1,‡}

Olig1 and Olig2 are closely related basic helix-loop-helix (bHLH) transcription factors that are expressed in myelinating oligodendrocytes and their progenitor cells in the developing central nervous system (CNS). Olig2 is necessary for the specification of oligodendrocytes, but the biological functions of Olig1 during oligodendrocyte lineage development are poorly understood. We show here that Olig1 function in mice is required not to develop the brain but to repair it. Specifically, we demonstrate a genetic requirement for Olig1 in repairing the types of lesions that occur in patients with multiple sclerosis.

The oligodendrocyte is the myelinating cell of the central nervous system (CNS) (1, 2). The appearance of these myelinating cells during evolution is thought to have enabled

the vertebrate nervous system to grow large and complex by allowing saltatory conduction of nervous impulses (3). A variety of demyelinating diseases exist in humans,

wherein the myelin sheaths are lost, usually through the death of mature oligodendrocytes. One principal example, multiple sclerosis (MS), affects roughly two and a half million people worldwide and is one of the most common causes of neurological disability in young adults (4–6). Typically, patients with MS present with a relapsing/remitting form of the disease, characterized by acute demyelinating episodes followed by the generation of new oligodendrocytes, remyelination, and functional recovery. However, remyelination is an inconsistent

¹Dana-Farber Cancer Institute, Harvard Medical School, Boston, MA 02115, USA. ²Cambridge Centre for Brain Repair and Department of Veterinary Medicine, University of Cambridge, Cambridge CB3 0ES, UK. ³Lineberger Comprehensive Cancer Institute, University of North Carolina, Chapel Hill, NC 27599, USA. ⁴Department of Pathology (Neuropathology), Albert Einstein College of Medicine, Bronx, NY 10461, USA.

*These authors contributed equally to this work.
 †Present address: Amgen Corporation, 1201 Amgen Court West, Seattle, WA 98119, USA.
 ‡To whom correspondence should be addressed. E-mail: charles_stiles@dfci.harvard.edu (C.D.S.); rjf1000@cam.ac.uk (R.J.M.F.)